A combined characterization of clusters in naturally aged Al–Cu–(Li, Mg) alloys using small-angle neutron and X-ray scattering and atom probe tomography

R. Ivanov, A. Deschamps, F. de Geuser

JOURNAL OF APPLIED CRYSTALLOGRAPHY

ISSN: 1600-5767
journals.iucr.org/j

A combined characterization of clusters in naturally aged Al–Cu–(Li, Mg) alloys using small-angle neutron and X-ray scattering and atom probe tomography

R. Ivanov, A. Deschamps and F. De Geuser

J. Appl. Cryst. (2017). **50**, 1725–1734

JOURNAL OF APPLIED CRYSTALLOGRAPHY
ISSN 1600-5767

A combined characterization of clusters in naturally aged Al–Cu–(Li, Mg) alloys using small-angle neutron and X-ray scattering and atom probe tomography

R. Ivanov, A. Deschamps and F. De Geuser*

Univ. Grenoble Alpes, CNRS, Grenoble INP, SIMAP, 38000 Grenoble, France. *Correspondence e-mail: frederic.de-geuser@simap.grenoble-inp.fr

Received 12 June 2017
Accepted 6 October 2017

Edited by G. Kostorz, ETH Zurich, Switzerland

Keywords: small-angle scattering; solute clusters; compositional fluctuations; Al–Cu alloys.

A new methodology for the characterization of solute clusters leading to compositional fluctuations is presented and discussed. The methodology makes use of contrast variation arising from a combination of small-angle scattering using neutrons and X-rays, and adapts a model for solute correlation to extract the chemistry and length scale of clustered states after quench and after natural ageing. In three subsets of the Al–Cu system, Cu-rich clusters are reported for all cases. The presence of Mg strongly enhances Cu clustering in the naturally aged state and results in more than double the number of clusters in the complex Al–Cu–Li–Mg system. The results are compared with those obtained using atom probe tomography.

1. Introduction

Certain aluminium alloys undergo natural ageing after they have been quenched from the solution treatment temperature. Guinier and Preston (Guinier, 1938; Preston, 1938) first reported natural ageing as being related to solute clustering on the atomic scale. Solute clustering describes the first stages of solute aggregation, in the form of solute-rich regions with no specific crystallographic structure. Ringer *et al.* (1996, 1997) reported Cu–Mg clusters as the cause of a rapid hardening mechanism observed by atom probe tomography (APT) in the Al–Cu–Mg system. Similarly, Starink *et al.* (2004) recorded strong exothermic reactions related to the formation of Cu–Mg clusters in differential scanning calorimetry (DSC) experiments. Deschamps *et al.* (2011) showed such clusters to have Guinier radii of 4.5 Å and Cu compositions between 25 and 45%, using a combination of small-angle X-ray scattering (SAXS) and NMR. Marceau and co-workers (Marceau, Sha, Ferragut *et al.*, 2010) pointed to these clusters having an Mg:Cu ratio $\gtrsim 2$ on the basis of APT and highlighted the importance of Mg as a potential vacancy stabilizer through the formation of vacancy–Mg complexes, as reported by Nagai *et al.* (2001). Furthermore, minor Mg additions have been shown to modify considerably the precipitation sequence and kinetics of complex commercial Al–Cu–Li alloys by changing the low-temperature microstructure formed during the early stages of ageing (Araullo-Peters *et al.*, 2014; Gumbmann *et al.*, 2016). Decreus *et al.* (2013) showed, using anomalous small-angle X-ray scattering (ASAXS), that Cu-rich clusters exist after natural ageing in an Al–Cu–Li–Mg alloy. As such, clustering is shown to be intimately related to the complex interactions between different solutes, and between the solutes and excess vacancies inherited from quenching from solution heat

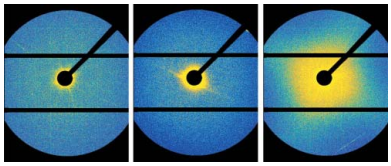

Table 1
SAS elemental sensitivity in aluminium alloys as defined by $(f_i - f_{Al})/f_{Al}$, with f_i and f_{Al} the scattering factors of element i and Al, respectively.

	Cu	Mg	Li
SAXS	1.23	−0.08	−0.77
SANS	1.23	0.55	−1.55

Table 2
Alloy compositions.

Alloy	Cu, at.% (wt%)	Li, at.% (wt%)	Mg, at.% (wt%)	Al	Mg/Cu, at.%
Al–Cu–Mg	1.1 (2.5)	N/A	1.7 (1.5)	Balance	1.55
Al–Cu–Li	1.5 (3.5)	3.5 (0.9)	N/A	Balance	0
Al–Cu–Li–Mg	1.5 (3.5)	3.5 (0.9)	0.45 (0.4)	Balance	0.3

treatment. It is therefore of interest to understand in more detail the respective interactions between Cu, Mg and Li in forming solute clusters during natural ageing. In the present paper, we will evaluate the cluster characteristics in three different alloys illustrating subsets of the Al–Cu system, namely an Al–Cu–Li alloy, an Al–Cu–Mg alloy and an Al–Cu–Li–Mg alloy.

Solute clusters are difficult to characterize directly, being of the same crystal structure as the host Al matrix and thus showing no sharp interface and only a minor composition contrast. Therefore, they have been mostly evaluated by indirect techniques, using DSC (Miao & Laughlin, 2000; Charai *et al.*, 2000; Starink, 2004), resistivity (Noble, 1968; Rosen *et al.*, 1982; Chobaut *et al.*, 2016), hardness or positron annihilation (Somoza & Dupasquier, 2003; Klobes *et al.*, 2008; Lay *et al.*, 2012). APT, giving access to the solute distribution on the atomic scale, has also been extensively used and has provided information on the type of solute correlations within the clusters and on their size distribution (Ringer *et al.*, 1997, 1998; Marceau, Sha, Ferragut *et al.*, 2010; Marceau *et al.*, 2012, 2013; Gault, de Geuser *et al.*, 2011). SAS techniques (SAXS with X-rays and SANS with neutrons) are well suited to evaluating the solute inhomogeneity on the near-atomic scale (Decreus *et al.*, 2013; De Geuser & Deschamps, 2012), giving access to information on the size of precipitates or clusters and on their quantity. This is classically the volume fraction for precipitates, although this term is more difficult to define in the case of clusters. Recently, Couturier *et al.* (2016) devised a methodology to characterize the composition fluctuations arising from Fe–Cr unmixing in a stainless steel from SAXS measurements. This methodology was successfully applied to characterize the amplitude and spatial extension of the composition fluctuations. In a multi-constituent system, however, a single SAXS measurement is insufficient to provide information on the clustering of several solutes, and contrast variation analysis is necessary to separate the contributions of the different solutes. ASAXS is classically used to evaluate the contribution of a specific solute by varying the X-ray beam energy close to the K edge of the element. The technique can be straightforward for high atomic number elements whose K edges are easily accessible, as shown by Lyon & Simon (1986) for unmixing of an Al–Zn–Ag system and by Marlaud *et al.* (2010) for clusters in Al–Zn–Cu–Mg. However, the K edges for Mg and (even worse) Li are not accessible by conventional synchrotron SAXS beamlines.

An alternative for contrast variation is to perform SAXS and SANS measurements correlatively. SAXS is sensitive to the electron density (which is related to the atomic number), while the SANS nuclear scattering cross section is not directly correlated to the position in the periodic table. In the case of dilute alloys, a measure of the sensitivity to a given element can be defined by $(f_i - f_{Al})/f_{Al}$, with f_i and f_{Al} the scattering factors of element i and Al, respectively. The values for Cu, Li and Mg are given in Table 1. It is clear from this table that, because Mg and Al have similar atomic numbers, SAXS is essentially blind to Mg clustering. This is much less the case for SANS. In favourable cases, their combination can be therefore expected to provide chemical information, as shown by Gerold (1977) on the miscibility gap in the Al–Zn–Mg system and by Ohnuma *et al.* (2009) on the characterization of oxide-dispersion steels. In combination with the analysis of the SAXS/SANS intensity using the model of Couturier *et al.* (2016), this contrast variation method will be used in the present case on all three alloys to provide a full quantification of the state of clustering. In addition, the information obtained from this correlative methodology will be further complemented by APT experiments, which give access to a direct spatial view of the solute fluctuations.

2. Materials and experiments

Alloys with the nominal compositions shown in Table 2 were provided as 27 mm thick plates by Constellium C-TEC, Voreppe, France. The material was homogenized at 773 K for 24 h, quenched and subsequently hot-rolled to 3 mm thickness at 623 K. For SANS no further thickness reductions were necessary and the samples were solution-treated at 773 K for 30 min, water-quenched, naturally aged where necessary and stored in liquid nitrogen before exposure to the beam. Samples for SAXS were prepared by grinding and polishing down to ∼300 µm, solution-treated at 773 K and water-quenched. Further thickness reduction down to 80 µm was achieved by polishing immediately after quench before exposure to the X-ray beam. Samples referred to as being in the 'as-quenched' (AQ) condition were exposed to room temperature for no longer than 5 min prior to SANS experiments and 15 min prior to SAXS experiments. Some of the samples were kept at room temperature (293 K) for 72 h after quench to allow for natural ageing to take place. These samples are referred to as 'naturally aged' (NA).

SAXS experiments were carried out on a laboratory setup using a Rigaku MicroMax-007 HF rotating anode with a Cu $K\alpha$ X-ray source (wavelength 1.52 Å) generating a beam with a cross section of 1 mm^2. Scattering data were collected using a Dectris PILATUS2 300K detector. The collected data were background corrected and normalized to absolute units using in-house scripts, with a glassy carbon sample as a secondary calibration standard (Huang *et al.*, 1993). For

comparison with SANS, we chose to use cm^{-1} rather than the units more conventionally used in SAXS (e $Å^{-3}$ or $Å^{-3}$), which requires a further normalization by the scattering cross section of an electron. The sample-to-detector distance was about 0.6 m, allowing the measurement of scattering vector magnitudes ranging between 0.02 and 0.5 $Å^{-1}$.

SANS measurements were performed on the D11 instrument at the Institute Laue–Langevin (ILL) in Grenoble, France, under proposal 1-01-142 (De Geuser *et al.*, 2015). A neutron wavelength of 5 Å was used, which is above the Bragg cut-off, removing any Bragg diffraction effects including double diffraction. Two distinct sample-to-detector distances were used to capture a wide range of scattering angles ($0.01 < q < 0.6$ $Å^{-1}$). The use of two positions required a displacement of the detector which lasted about 1 min. Thus, in order to increase the time resolution of the SANS measurements on the AQ samples, only the shortest distance was used. All experimental data were background corrected, normalized to absolute units and azimuthally averaged using the *Graphical Reduction and Analysis SANS Program* package (*GRASP*; https://www.ill.eu/instruments-support/instruments-groups/groups/lss/grasp/home/).

APT samples were prepared by cutting small rods (~0.3 × 0.3 × 15 mm) from the NA material. Final tip specimens for APT analysis were obtained using a standard two-stage electropolishing technique (Larson *et al.*, 2013) in 2% perchloric acid in 2-butoxyethanol at 15 V. AQ samples were not tested because of the long dwell time between electropolishing and APT data acquisition. In addition, since only a limited APT access time was awarded through a METSA call for proposals, only the Al–Cu–Mg and Al–Cu–Li–Mg alloys were tested. APT experiments were carried out using a Cameca LEAP 4000 instrument at Rouen University. The temperature of the sample was maintained at 40 K under ultrahigh vacuum of the order of 8×10^{-11} Torr (1 Torr = 133.322 Pa) during the experiments. Evaporation was achieved in electric mode using a pulse with an amplitude of 20% of the DC voltage applied at 200 kHz repetition. The collected data were processed with the Cameca *IVAS* software package. Volume reconstructions were done following advanced techniques described and reviewed elsewhere (Gault *et al.*, 2008; Gault, Haley *et al.*, 2011; Vurpillot *et al.*, 2013). Solute-enriched poles were observed and removed from the volumes used for radial distribution function (RDF) calculations.

3. Data interpretation

3.1. General framework

SAS experiments are measurements of the fluctuations of scattering factor density and provide excellent statistical information owing to the large volumes analysed. These fluctuations originate from features in the sample such as precipitates or clusters. The use of different sources of radiation permits changes in the nature of the scattering factors and in turn provides complimentary information from fluctuations in the same system. When using X-rays, the scattering signal is sensitive to variations in electron density and therefore provides information on the chemical fluctuations *via* the atomic number. Elements of atomic number close to the host solution, *e.g.* Si or Mg as solutes in Al, give low scattering, whereas elements with large differences, such as Cu, result in stronger scattering. The nuclear scattering of neutrons is not related to atomic number, allowing for a scattering experiment in which elements with similar atomic number can still generate contrast, *e.g.* Mg in Al. A combination of scattering experiments with different sources provides a method for characterizing the fluctuations on the basis of their chemical nature.

In an isotropic system of average scattering factor density $\overline{\rho}$, the intensity $I(q)$ arising from a fluctuation in scattering factor density $\eta = \rho - \overline{\rho}$ can be written (Porod, 1982) as

$$I(q) = \int_0^\infty 4\pi r^2 \gamma(r) \frac{\sin(qr)}{qr}\, \mathrm{d}r, \tag{1}$$

where q is the scattering vector magnitude and $\gamma(r)$ is the so-called correlation function introduced by Debye & Bueche (1949):

$$\gamma(r) = \langle \eta(\mathbf{r}_1)\eta(\mathbf{r}_2)\rangle \quad \text{with} \quad r = |\mathbf{r}_1 - \mathbf{r}_2| = \text{constant}. \tag{2}$$

$\gamma(r)$ is the autocorrelation of the scattering density fluctuation and is related to the SAS intensity through a Fourier transform. It can be rewritten as

$$\gamma(r) = \overline{\eta^2}\gamma_0(r) \quad \text{with} \quad \gamma_0(0) = 1, \tag{3}$$

where $\gamma_0(r)$ is the normalized correlation function. In the absence of long-range order (other than that of the underlying crystal giving rise to Bragg peaks), both γ and γ_0 go to zero for large r. By definition, $\gamma(0) = \overline{\eta^2}$, *i.e.* the mean-squared fluctuation of the scattering factor density.

When considering concentration fluctuations (with constant atomic volume), the normalized correlation function $\gamma_0(r)$ is technique independent and essentially geometric (*i.e.* it is characteristic of the shape of the objects and their interaction, if any). The mean-squared fluctuation, however, depends on what the technique is actually probing (electrons for X-rays, nuclear scattering length for neutrons, atoms for APT). Its expression will be discussed further in this paper.

Provided that the intensity is known over a wide enough range, the correlation function can be obtained by an inverse Fourier transform,

$$\gamma(r) = \frac{1}{2\pi^2} \int_0^\infty I(q)\, q^2 \frac{\sin(qr)}{qr}\, \mathrm{d}q. \tag{4}$$

In particular, for $r = 0$

$$\overline{\eta^2} = \frac{1}{2\pi^2} \int_0^\infty I(q)\, q^2\, \mathrm{d}q. \tag{5}$$

Because this integral is always equal to the mean-squared fluctuation of the scattering factor density, irrespective of the shape of the features, it is often called the invariant.

This framework gives the relationship between a description of the chemical fluctuations in real space [$\gamma(r)$] and the intensity they give rise to in reciprocal space [$I(q)$]. The correlation function contains information on the correlations between the positions of solute atoms. As shown by Couturier *et al.* (2016), it is closely related to the radial distribution function (RDF), which is a standard tool to describe the solute fluctuations in APT (De Geuser, 2005; Sudbrack *et al.*, 2006).

3.2. The model for the correlation function $\gamma(r)$

The concept of a correlation function is very general and also holds for a two-phase model where one can distinguish between a matrix and precipitates (including non-particulate systems) or for a system where the concentration fluctuations are diffuse and can only be described by concentration wavefunctions.

In the study of precipitation of metals, the interpretation models are usually built up from the calculated correlation function (or SAS intensity) of a single object (precipitate) embedded in a matrix and generalized for an assembly of objects, with or without interactions. The correlation functions (and associated SAS signal) of simple precipitate shapes (sphere, flat cylinder, long cylinder *etc.*) can be found in the literature (Deschamps & De Geuser, 2011). They can be adapted for a particular system to account for non-uniform solute distributions in the object, abrupt or diffuse interfaces, size distributions, or interference between neighbouring objects.

These additional parameters lead to modification of the form factor, integration of a size dispersion function and use of an interparticle structure factor, all of which are interdependent, so the complete model can be complex. Although this approach has proven successful in numerous studies concerning well defined precipitates in metallic systems (Dorin *et al.*, 2014; De Geuser & Deschamps, 2012), the study of clustering combines all these difficulties: (i) ill defined shape, (ii) diffuse concentration with no clear interface, (iii) wide size dispersion, and (iv) large quantity and number density implying interference between objects. The combination of these aspects calls for a more statistical description of the concentration fluctuations. Following Couturier *et al.* (2016), we use a similar approach to that of Teubner & Strey (1987), who built their description of the scattering from microemulsions upon a statistical description of the correlation function. The use of an exponentially decaying correlation (with a correlation length ξ) represents the direct correlation between the domains (clusters) and is general enough to capture the effect of a wide size dispersion and diffuse interfaces. This should be modulated by an oscillating function capturing the interaction between the domains. Oppositely to Teubner & Strey (1987), we used a cosine function for that purpose, which, in our experience, better reproduces the experimental data in metallic systems. This model has already been successfully applied to the early stages of solid solution unmixing in an Fe–Cr based alloy (Couturier *et al.*, 2016) and can be written as

$$\gamma(r) = \overline{\eta^2}\gamma_0(r) = \overline{\eta^2}\exp\left(-\frac{r}{\xi}\right)\cos\left(\frac{2\pi}{\lambda}r\right), \tag{6}$$

where the correlation length ξ is a measurement of the size of the clusters and the modulation periodicity λ can be related to the distance between them. If λ is much larger than ξ, the objects are non-interacting. Smaller values of λ indicate much more numerous objects, *i.e.* a higher quantity. The constant $\overline{\eta^2}$ is the mean-squared fluctuation or scattering invariant.

3.3. Corresponding intensity $I(q)$

The model used for $\gamma(r)$ can be incorporated into equation (1), the integral of which can be analytically calculated. The expression for the intensity gives

$$I(q) = \overline{\eta^2}\frac{8\pi\xi^3}{\left(1+\xi^2q^2\right)^2}S(q,\lambda,\xi). \tag{7}$$

The structure factor $S(q,\lambda,\xi)$ is such that its value is 1 when λ is large (small fraction). For decreasing λ, $S(q,\lambda,\xi)$ creates an interference peak at intermediate q before reaching 1 for larger q. $S(q,\lambda,\xi)$ can be written as

$$\begin{aligned} S(q,\lambda,\xi) = &\left\{\lambda^4\left(1+\xi^2q^2\right)^2\left[\lambda^4\xi^4q^4+\left(8\pi^2\lambda^2\xi^2+2\lambda^4\right)\xi^2q^2\right.\right. \\ &\left.\left.-48\pi^4\xi^4-8\pi^2\lambda^2\xi^2+\lambda^4\right]\right\} \\ &\Big/\left[\left(\lambda^2\xi^2q^2-4\pi\lambda\xi^2q+4\pi^2\xi^2+\lambda^2\right)^2\right. \\ &\left.\times\left(\lambda^2\xi^2q^2+4\pi\lambda\xi^2q+4\pi^2\xi^2+\lambda^2\right)^2\right]. \end{aligned} \tag{8}$$

The positivity of the intensity imposes that $\lambda > (12)^{1/2}\pi\xi$. The correlation length ξ is linked to the distance between solutes within a cluster and is hence a measure of the fluctuation size

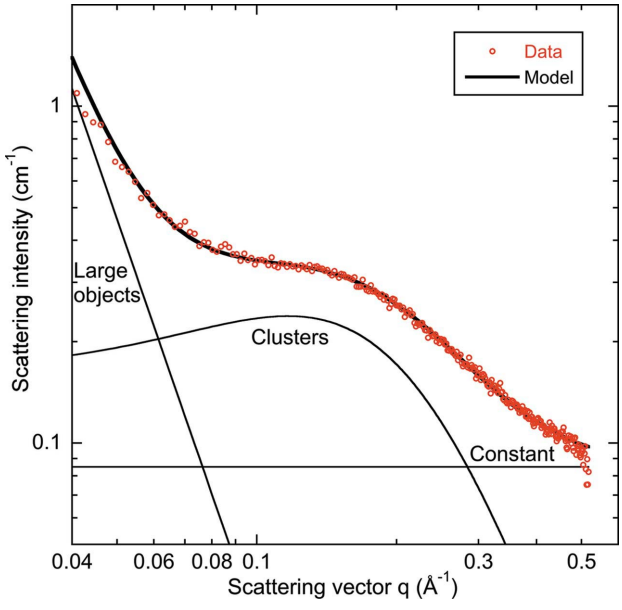

Figure 1
The scattering profile (red circles) for naturally aged Al–Cu–Li–Mg alloy and a corresponding model fit (thick black line) incorporating the scattering intensity contributions due to clusters, large objects and a background constant (thin black lines).

in real space. For the reader familiar with existing SAS interpretation models, it is interesting to note the following:

(i) In the absence of interaction between the solute-rich zones [*i.e.* $S(q, \lambda, \xi) = 1$ and $\lambda \cong \infty$], $I(q)$ respects the Guinier approximation with a Guinier radius R_g of

$$R_g = 6^{1/2}\xi, \tag{9}$$

so that R_g is about 2.45 times the correlation length.

(ii) $I(q)$ follows the Porod law at high q in the sense that its high-q asymptote has the k_p/q^4 (with k_p a constant) behaviour which is typical of (but not exclusive to) sharp interface particles. We can thus define the Porod radius as

$$R_p = \frac{3Q_0}{\pi k_p} = \frac{3}{4}\xi, \tag{10}$$

where $Q_0 = \int_0^\infty Iq^2\,\mathrm{d}q = 2\pi^2\overline{\eta^2}$. This model was derived without any shape or size distribution in mind. It is nevertheless interesting to note that $R_p \ll R_g$ is typical of a broad size distribution in the case of spherical particles (Deschamps & De Geuser, 2011).

Fig. 1 shows an example of the resulting intensity function fitted to the SAXS pattern obtained from a naturally aged Al–Cu–Li–Mg alloy. In addition to the described contribution of the clusters, we also added a Porod-type contribution of large objects (*e.g.* dispersoids) proportional to $1/q^4$, as well as a constant contribution accounting for the solid-solution Laue scattering and other incoherent sources of signal (incoherent nuclear scattering for neutrons, fluorescence for X-rays).

3.4. Expression of the mean-squared fluctuation $\overline{\eta^2}$

While $\gamma_0(r)$ describes the geometric distribution of the fluctuations/clusters, independent of their chemical nature, $\overline{\eta^2}$ is a function of their chemical content. As such, it is technique dependent, since each technique has its own sensitivity to each element (see Table 1). The contribution of each element should be explained. Let us start with a binary Al–Cu system, for which we assume the atomic volume Ω to be constant. Since $\eta = \rho - \overline{\rho}$, we can write $\overline{\eta^2}$ as

$$\begin{aligned}\overline{\eta^2} = \langle(\rho - \overline{\rho})^2\rangle &= \frac{\left(f_{Al} - f_{Cu}\right)^2}{\Omega^2}\left\langle\left(c_{Cu} - \overline{c_{Cu}}\right)^2\right\rangle \\ &= \frac{\left(f_{Al} - f_{Cu}\right)^2}{\Omega^2}\overline{\Delta c_{Cu}^2}.\end{aligned} \tag{11}$$

where f_i is the (technique-dependent) scattering factor. $\overline{\Delta c_{Cu}^2}$ is the mean-squared concentration fluctuation (independent of the technique). It has no units as it is a squared concentration. Although its definition is more general, $\overline{\Delta c_{Cu}^2}$ is such that, in a two-phase model with a well defined volume fraction f_v,

$$\overline{\Delta c_{Cu}^2} = \left\langle\left(c_{Cu} - \overline{c_{Cu}}\right)^2\right\rangle = f_v(1 - f_v)\left(c_{Cu}^p - c_{Cu}^m\right)^2, \tag{12}$$

with c_i^p and c_i^m the concentrations of element i in the precipitate (*e.g.* the scattering objects) and the matrix, respectively. The mean-squared fluctuation, because it is related to the scattering invariant (*i.e.* to the integrated intensity), is traditionally used in SAS studies as a measure of the number of objects. In fact, equation (12) shows that it is related to the volume fraction through a contrast term $(c_{Cu}^p - c_{Cu}^m)^2$. If we can assume that this contrast term is constant, then the integrated intensity is indeed a measurement of the number of scattering objects. In the early stages of solid-solution decomposition, and when we only consider solute clusters, it is reasonable to release the assumption of fixed chemistry of the phases. In this case, the mean-squared concentration fluctuation $\overline{\Delta c_{Cu}^2}$ is not directly a measurement of the advancement of the reaction, since it may have a non-monotonic behaviour as more and more solutes are involved in the clusters. This can be understood by looking at the two-phase model case [equation (12)] and imagining a fixed number of objects. If the number of solute atoms incorporated into clusters increases more slowly than the volume of the objects (*i.e.* the cluster concentration decreases) then the integrated intensity decreases. However, the reaction has arguably advanced since more solute atoms are involved.

Perhaps a better measurement of the advancement of the reaction would be the total number of atoms involved in the clusters. While this is not measured by a scattering experiment, one may consider the mean-squared number of excess solute atoms. This is similar to what was described by Porod (1982) as the squared number of excess electrons by considering the intensity at $q = 0$ of a single object. At $q = 0$, where all secondary waves are in phase, the intensity is simply the sum of the squared numbers of excess electrons. We can drop the $(f_{Al} - f_{Cu})^2$ term to define the mean-squared number of excess solute atoms $\overline{\Delta n_{Cu}^2}$. This is related to the mean-squared concentration fluctuation through

$$\overline{\Delta n_{Cu}^2} = \frac{\overline{\Delta c_{Cu}^2}}{\Omega^2}\,\nu_c, \tag{13}$$

where ν_c is a correlation volume which is equal to $8\pi\xi^3$ in the model of equations (1) and (7). Finally,

$$\overline{\Delta n_{Cu}^2} = \frac{8\pi\xi^3}{\Omega^2}\,\overline{\Delta c_{Cu}^2}. \tag{14}$$

This solves the possible ambiguity of the mean-squared concentration fluctuation: when the mean-squared number of excess solute atoms $\overline{\Delta n_{Cu}^2}$ increases, it means that more solutes are involved in the clusters. It is the sum of the squares of the number of solutes in excess, per unit volume.

We should now consider the case of a ternary system, *e.g.* Al–Cu–Mg. The mean-squared fluctuation now consists of three terms, the Al–Cu interaction term, the Al–Mg interaction term and the Cu–Mg cross term,

$$\begin{aligned}\overline{\eta^2} = &\frac{\left(f_{Al} - f_{Cu}\right)^2}{\Omega^2}\overline{\Delta c_{Cu}^2} + \frac{\left(f_{Al} - f_{Mg}\right)^2}{\Omega^2}\overline{\Delta c_{Mg}^2} \\ &+ 2\frac{\left(f_{Al} - f_{Cu}\right)\left(f_{Al} - f_{Mg}\right)}{\Omega^2}\overline{\Delta c_{CuMg}^2}.\end{aligned} \tag{15}$$

The cross term explains how there can be negligible signal even for significant clustering if $(f_{Al} - f_{Cu})$ and $(f_{Al} - f_{Mg})$ are of opposite sign. Their presence in the same clusters has compensating effects on the SAS intensity. Since we have

assumed a single type of fluctuation or cluster, the mass balance imposes

$$\overline{\Delta c^2_{\mathrm{CuMg}}} = \left(\overline{\Delta c^2_{\mathrm{Cu}}}\ \overline{\Delta c^2_{\mathrm{Mg}}}\right)^{1/2}. \quad (16)$$

Finally, in a ternary Al–Cu–Mg alloy, our model leaves four parameters to be determined: ξ, λ, $\overline{\Delta c^2_{\mathrm{Cu}}}$ and $\overline{\Delta c^2_{\mathrm{Mg}}}$. In a single SAS experiment (SAXS or SANS), $\overline{\Delta c^2_{\mathrm{Mg}}}$ and $\overline{\Delta c^2_{\mathrm{Mg}}}$ are combined into a single $\overline{\eta^2}$ term depending on the scattering factors. We thus used combined SAXS and SANS which were simultaneously fitted to the model using the same four parameters ($\overline{\Delta c^2_{\mathrm{Cu}}}$, $\overline{\Delta c^2_{\mathrm{Mg}}}$, ξ and λ) for both experiments.

3.5. The radial distribution function from atom probe tomography and the correlation function

The chemical and spatial information obtained from APT experiments can be analysed statistically to calculate the partial pair correlation function from the radial distribution function (RDF) for solutes present in the dataset (De Geuser *et al.*, 2006; Sudbrack *et al.*, 2006). The pair correlation function is a measurement of the probability of finding a specific pair of atoms at a distance r and is hence a good way of describing solute clustering. Analysis of sufficiently large APT datasets provides good statistics on the correlation of solutes and has been used to estimate solute ratios in clusters (De Geuser *et al.*, 2006). As derived from the RDF, the partial pair correlation function $g_{i-j}(r)$ between element i and element j can be defined as the average local concentration in element j around atoms of i at a given distance r normalized by the mean concentration of j:

$$g_{i-j}(r) = \frac{c_{i-j}(r)}{\overline{c_j}}. \quad (17)$$

The method may be influenced by some of the artefacts associated with the experimental procedure of APT, such as the (anisotropic) spatial resolution; however, their qualitative properties should not be affected. As shown by Couturier *et al.* (2016), the correlation functions for APT data and SAS data are both measurements of the same fluctuation of solute within the sample. The relationship between the correlation function introduced in the previous sections and the APT RDF can be written as

$$g_{\mathrm{Cu\text{-}Cu}}(r) - 1 = \gamma_{\mathrm{APT}}(r) = \frac{\overline{\Delta c^2_{\mathrm{Cu}}}}{c^2_{\mathrm{Cu}}}\,\gamma_0(r), \quad (18)$$

where $\gamma_{\mathrm{APT}}(r)$ is simply the APT Cu–Cu pair correlation extracted from the RDF minus 1 to allow for a zero value for large r. The value at $r = 0$ gives the mean-squared concentration fluctuation.

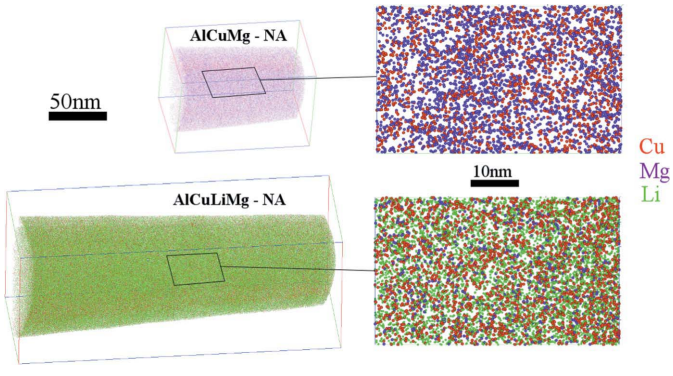

Figure 2
(Left) Atom probe volumes of naturally aged Al–Cu–Mg and Al–Cu–Li–Mg alloys, and (right) their corresponding two-dimensional sections

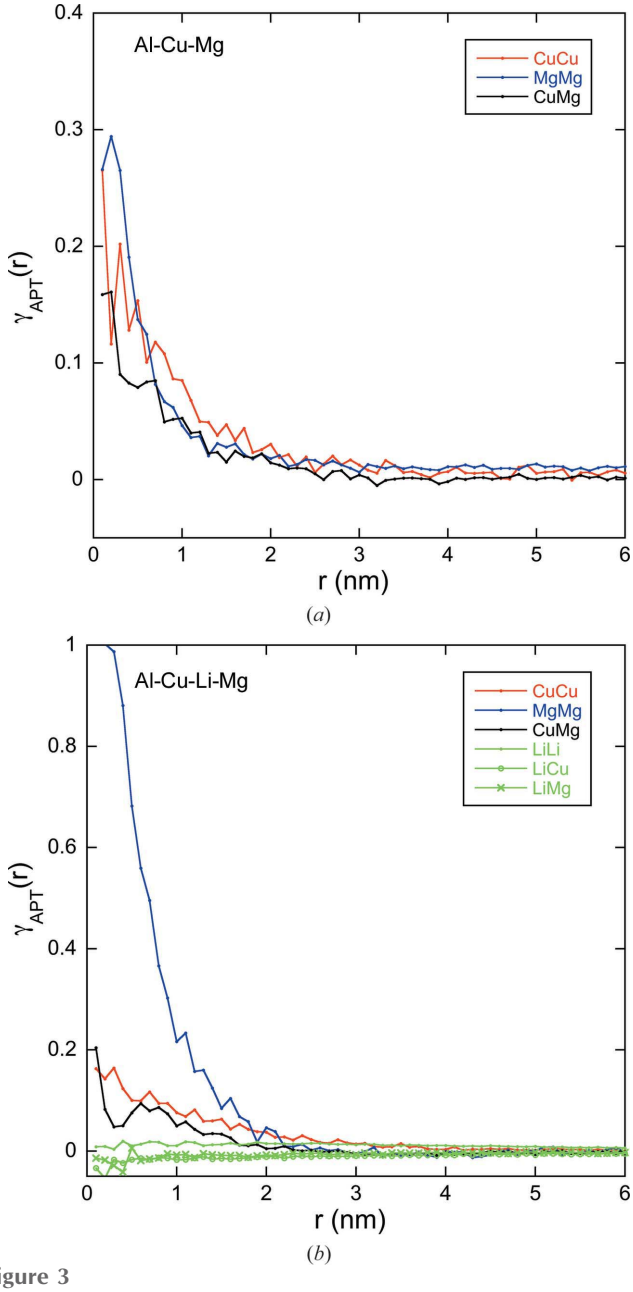

Figure 3
Amplitudes of the radial distribution functions for solute pairs in (*a*) Al–Cu–Mg and (*b*) Al–Cu–Li–Mg alloys in the naturally aged condition. Deviations from zero are indicative of solute correlation.

4. Results

4.1. Solute correlations obtained from APT

The volumes of the Al–Cu–Mg and Al–Cu–Li–Mg alloys in the NA condition analysed by APT are shown in Fig. 2. Microstructural features (such as grain boundaries or larger constituent particles) are not contained in the volumes and hence they are good representations of the NA solid solution. A closer look at the solute distribution is provided by the two-dimensional sections. The distributions of solutes appear to be non-random, with some correlation existing between solutes. Nevertheless, areas of high solute density are not easy to identify with certainty. We calculate the RDFs of all solutes in order to characterize the non-random distribution of solute in the volumes.

The auto-correlation functions $\gamma_{\rm APT}(r)$ calculated from APT are presented in Fig. 3. For the Al–Cu–Mg alloy in the NA condition, clustering of solutes is statistically significant, as shown by increased correlation of both Cu and Mg atoms and their cross-correlation in Fig. 3(*a*). The correlation data indicate an exponential decay with respect to distance. The correlation becomes negligible for distances larger than 2 nm, suggesting the presence of very small domains.

For the Al–Cu–Li–Mg alloy, the correlation functions calculated for all possible solute pairs in the NA condition are shown in Fig. 3(*b*). The Mg–Mg correlation is shown to be the strongest, with $\gamma_{\rm APT}(0)$ values estimated to be above unity, suggesting that the Mg atoms are strongly correlated at distances below 2 nm. The Cu–Cu and Cu–Mg correlations are weaker than that observed for Mg. Li-related correlations seem compatible with a random distribution [$\gamma_{\rm APT}(r) \equiv 0$] in all cases. The lack of Li correlation (clustering) allows for the interpretation of the small-angle scattering without an Li-related signal.

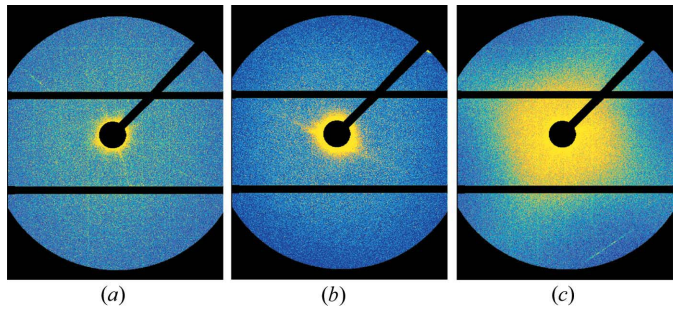

Figure 4
Raw two-dimensional scattering data as captured during SAXS experiments for naturally aged (*a*) Al–Cu–Li, (*b*) Al–Cu–Mg and (*c*) Al–Cu–Li–Mg alloys.

4.2. Experimental results from SANS and SAXS

The raw SAXS two-dimensional patterns are shown in Fig. 4. Their corresponding radially averaged SAXS and SANS one-dimensional scattering profiles are shown in Fig. 5 for all alloys in the AQ and NA states. In all cases, the SANS data are of an order of magnitude lower intensity compared with the SAXS data because of the lower scattering cross section of neutrons. The SANS setup also has a slightly lower q range, so that the large-object Porod-type contribution is not always detected in SANS.

The Al–Cu–Li alloy shows only small differences between the AQ and NA conditions (Fig. 5*a*), evidencing the small change to clusters during natural ageing. The SANS curve for this alloy is predominantly composed of a flat constant and a limited increase in intensity in the Porod region for scattering from large objects, as described in Fig. 1. This alloy shows a somewhat larger intensity in SAXS, suggesting some degree of clustering of Cu.

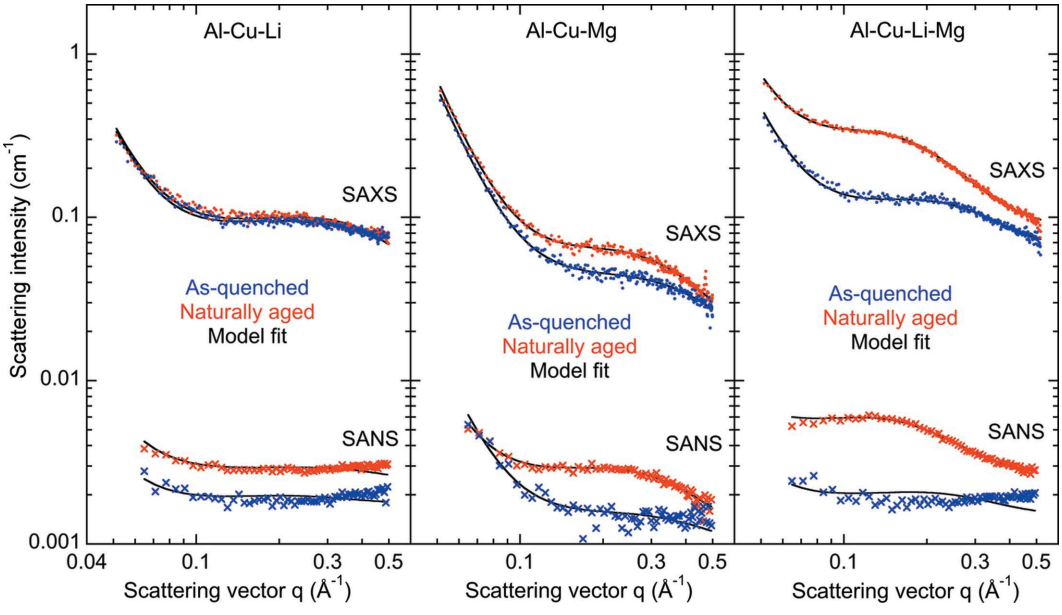

Figure 5
Radially averaged profiles of the scattering intensity collected during SAXS (filled circles) and SANS (crosses) experiments for (*a*) Al–Cu–Li, (*b*) Al–Cu–Mg and (*c*) Al–Cu–Li–Mg alloys. Data for the as-quenched (blue) and naturally aged (red) conditions are shown. Black lines indicate model fits in each case.

Table 3
Concentration fluctuations measured by fitting combined data from SAXS and SANS experiments.

Alloy	$\overline{\Delta c^2_{Cu}}$ ($\times$10000)	$\overline{\Delta c^2_{Mg}}$ ($\times$10000)	$\overline{\Delta n^2_{Cu}}$ (nm^{-3})	$\overline{\Delta n^2_{Mg}}$ (nm^{-3})	Mg/Cu	ξ (Å)	λ (Å)
Al–Cu–Li AQ	52 ± 36		5.3 ± 2.0			2.5 ± 1.0	38 ± 11
Al–Cu–Li NA	35 ± 25		4.8 ± 1.0			2.7 ± 0.7	43 ± 11
Al–Cu–Mg AQ	54 ± 17	25 ± 46	4.6 ± 0.6	1.9 ± 3.5	0.70	2.2 ± 0.2	36 ± 2.0
Al–Cu–Mg NA	41 ± 9.0	137 ± 31	9.9 ± 1.0	34 ± 11	1.82	3.0 ± 0.3	42 ± 1.0
Al–Cu–Li–Mg AQ	63 ± 44	1 ± 5.0	10.2 ± 1.4	0.1 ± 0.5	0.13	2.9 ± 1.0	44 ± 4.5
Al–Cu–Li–Mg NA	30 ± 0.4	5 ± 0.25	38.9 ± 0.6	7.1 ± 0.14	0.42	5.2 ± 0.05	72 ± 0.5

Alloys containing Mg show very different curves in the AQ and NA conditions, whether observed by SAXS or SANS, evidencing the occurrence of clustering during natural ageing. In the AQ condition, the SANS profiles are flat (Figs. 5*b* and 5*c*), whereas a small but significant SAXS intensity is recorded. The higher sensitivity of X-rays to Cu suggests that the initial clustering in the AQ state is dominated by Cu. After natural ageing, a large scattering signal appears in both alloys with both experimental techniques. The relative increase in SANS intensity is larger than that of SAXS intensity, suggesting the clusters have a higher concentration of Mg in the NA condition. The shape of the profiles is similar in SAXS and SANS and will be more precisely evaluated when modelling the SAS signal. Nevertheless, this similarity is compatible with our model using a single type of concentration fluctuation.

The comparison between the Al–Cu–Li (Fig. 5*a*) and the Al–Cu–Li–Mg (Fig. 5*c*) alloys, whose composition difference is only 0.4 at.% Mg, is particularly interesting. The Al–Cu–Li alloy presents only a very small amount of clustering in the AQ condition which does not evolve much during 3 d of natural ageing. When adding a small amount of Mg (which does not give contrast with X-rays), a dramatic change in the scattering is observed. This means that the addition of a small amount of Mg to Al–Cu–Li provokes a major change in the clustering behaviour of the Cu atoms.

4.3. Application of the model to SAXS and SANS data

In addition to the experimental data for SANS and SAXS, Fig. 5 also shows the model fitted to the data. The agreement is generally excellent, except for the large-q range of some SANS patterns where the clustering signal is very low and the SANS signal seems to increase slightly. Table 3 shows the values of the mean-squared concentration fluctuation ($\overline{\Delta c^2_{Cu}}$ and $\overline{\Delta c^2_{Mg}}$), the mean-squared number of excess solutes ($\overline{\Delta n^2_{Cu}}$ and $\overline{\Delta n^2_{Mg}}$), the correlation length ξ and the interaction length λ. We also show in Table 3 the cluster Mg/Cu ratio, estimated by

$$\frac{Mg}{Cu} = \left(\frac{\overline{\Delta c^2_{Mg}} + c^2_{Mg}}{\overline{\Delta c^2_{Cu}} + c^2_{Cu}} \right)^{1/2}. \quad (19)$$

In addition to the parameter values, Table 3 shows an estimation of the uncertainties on the obtained parameters. This estimation was obtained by repeating the fit with 100 different random sets of initial guesses of parameters, in order to make sure we explored the complete parameter space. If this procedure were to result in very different values for a parameter, it would mean the amount of information is too low to determine this parameter.

5. Discussion

Choosing to analyse the solute distribution in the NA condition as observed by APT using RDF gives information on its non-random nature which can be argued to appear visually in Fig. 2. A benefit of using RDFs calculated from equation (15) is that they do not require assumptions such as a minimum cluster size, a minimum distance between solute atoms or an iso-concentration interface to identify a cluster. RDFs are calculated on large volumes and are considered as averages of the ensembles, with errors arising only from the method used to collect the data. As such, using RDFs is a purely statistical approach and holds valid for domains with diffuse interfaces and variable composition and size, which is likely to be the case for clusters. Furthermore, the average nature of RDFs grants the ability to compare them directly with auto-correlations calculated from an interpretation model for the intensity of SAS. The fact that Li shows very a low correlation with itself and other solutes (Fig. 3) in the APT data suggests that its distribution is near random. Such a distribution of Li will not give rise to scattering factor fluctuations when observed by SAS and hence allows for Li to be dropped from the interpretation of SAS intensity.

Characterization of the distribution of solute using SAS provides global average data which are visually rich and azimuthal averaging intuitively shows changes between the AQ and NA conditions (Fig. 5). Further information can be accessed by making some assumptions necessary to adopt an interpretation framework. The most global assumption is that of a constant atomic volume, Ω, which greatly simplifies the calculation of differences in scattering factor density. The coherence of the solute domains studied means that the lattice strains they impose are low and make a constant volume a good approximation. Having this in mind, the model proposed by Couturier *et al.* (2016) is dependent on only three parameters which hold physical meaning. The relationship between these parameters and the physical properties of solute clusters is discussed below.

The correlation length ξ, being a measurement of the mean distance at which solutes are encountered in a domain, is characteristic of the mean size of the objects. In the initial stages of solute clustering all alloys have very small correlation lengths (between 2 and 3 Å), indicating that the clusters are small. This corresponds to Guinier radii of about 5–7 Å. The change in scattering intensity between AQ and NA states for Al–Cu–Mg and Al–Cu–Li–Mg alloys results in larger correlation lengths, which in turn mean larger clusters (ξ up to 5.2 Å, corresponding to R_g of about 13 Å).

The modulation periodicity λ allows the model to capture possible interaction between domains. It can be visualized as the concept of excluded volume when considering precipitation in a two-phase model where two precipitates cannot be found on the same point of the lattice. As such the periodicity λ is related to the average distance between domains. The relationship between λ and ξ is linked through the correlation volume v_c and the number density of domains. However, owing to the global nature of SAS this relationship cannot be separated without assumptions.

The third and final parameter of the interpretation model is the mean-squared fluctuation, η^2, which is a constant dependent only on the measurement technique. When normalized by the respective differences of the scattering factors it returns the mean-squared fluctuation in composition, $\overline{\Delta c_i^2}$. Furthermore, $\overline{\Delta c_i^2}$ grants access to the mean-squared number of excess solutes, $\overline{\Delta n_i^2}$, which is a measurement of the progress of a reaction.

The interpretation model that we have introduced here has the advantage of being defined in both direct and reciprocal space, allowing for fitting of both SAS and APT results. This should provide a direct quantitative comparison between the two techniques, as has already been shown successfully (De Geuser *et al.*, 2014; Couturier *et al.*, 2016). The fitting (not shown here) of the APT RDF using equations (18) and (6) has been attempted but the quantitative agreement with SAS has not proved successful. It is easy to see in Fig. 3 that the correlations extend further than the values given by SAS (Table 3). The correlation lengths found by APT are in the region of 7 Å, whereas SAS gives a range of 3–5 Å. Similarly, the concentration fluctuations observed on the APT RDF fit are systematically much smaller than those found by SAS. The most plausible explanation is that the effective spatial resolution of APT (*i.e.* the local element-specific radial spatial resolution) does not allow the resolution of those clusters/fluctuations at their actual size, as has already been observed by Couturier *et al.* (2016). The resolution would then 'flatten' the fluctuations, which would consequently be detected not only with a larger correlation length but also with a lower concentration fluctuation (by conservation). This gives some important insight into a possible synergy between the two techniques, and further direct comparisons of SAS and APT performed on microstructures of different scales may provide a valuable benchmark for the effective spatial resolution and detection efficiency of APT.

The use of the interpretation model [equation (6)] with the calculated parameters presented in Table 3 effectively captures the intensity of SAS experiments (Fig. 5) in all cases. In the Mg-free alloy, no significant evolution is observed during natural ageing. However, in the two Mg-containing alloys, natural ageing results in a strong increase in the number squared of excess solute (both Cu and Mg), the correlation length and the periodicity. The Mg/Cu ratio calculated through combined SAS experiments is in excellent agreement with previously reported solute ratios from APT experiments on the same alloy (Marceau, Sha, Lumley & Ringer, 2010). The lower Mg/Cu ratio in the Al–Cu–Li–Mg alloy can be related to the lower concentration of Mg. Nevertheless, the addition of only 0.45 at.% Mg to the Al–Cu–Li system results in profound changes to the clustering behaviour, in particular of Cu, which is worth further investigation. A forthcoming publication will be devoted to the kinetics of cluster formation with the aim of elucidating this effect.

6. Conclusions

We have successfully developed a methodology for characterizing the state of solute clustering in aluminium alloys. The complimentary interpretation of SAXS, SANS and APT results has been facilitated by the use of an interpretation model which provides crucial information on the clusters in the system. The main points can be summarized as follows:

(i) The non-random solid solutions of aluminium-containing solute clusters can be effectively characterized by statistical methods.

(ii) Considering clusters as fluctuations in the solute concentration has been shown to yield agreement between APT and SAS techniques.

(iii) In the as-quenched condition, some Cu-rich clusters are already present in the alloys (Fig. 5 and Table 3).

(iv) A significant change in the cluster state occurs between the as-quenched and naturally aged conditions for alloys containing Mg (Fig. 5 and Table 3).

(v) The chemical analysis reveals a drastic increase in the number of Mg atoms involved in clusters in the naturally aged state (Fig. 5 and Table 3).

(vi) The drastic increase in the number of Cu-rich clusters on the addition of Mg to Al–Cu–Li is strong evidence that Mg positively affects Cu clustering.

Acknowledgements

The authors would like to thank Dr Robert Cubitt for his help with the SANS experiments. The authors would also like to thank Dr Williams Lefebvre and Dr Ivan Blum for their help in the acquisition and interpretation of the APT data. We thank Dr Christophe Sigli for his help and support.

Funding information

The authors acknowledge the SANS beam time obtained through an ILL Call for Proposals (doi:10.5291/ILL-DATA.1-01-142). The authors acknowledge financial support from the CNRS-CEA 'METSA' French network (FR CNRS 3507) for the APT experiments conducted on the IRMA GPM platform. We also acknowledge financial support from Constellium C-Tec.

References

Araullo-Peters, V., Gault, B., de Geuser, F., Deschamps, A. & Cairney, J. M. (2014). *Acta Mater.* **66**, 199–208.
Charai, A., Walther, T., Alfonso, C., Zahra, A.-M. & Zahra, C. Y. (2000). *Acta Mater.* **48**, 2751–2764.
Chobaut, N., Carron, D. & Drezet, J.-M. (2016). *J. Alloys Compd.* **654**, 56–62.

Couturier, L., De Geuser, F. & Deschamps, A. (2016). *Mater. Charact.* **121**, 61–67.
Debye, P. & Bueche, A. M. (1949). *J. Appl. Phys.* **20**, 518–525.
Decreus, B., Deschamps, A., De Geuser, F., Donnadieu, P., Sigli, C. & Weyland, M. (2013). *Acta Mater.* **61**, 2207–2218.
De Geuser, F. (2005). PhD thesis, University of Rouen, France, https://tel.archives-ouvertes.fr/tel-00077980.
De Geuser, F., Cubitt, R., Deschamps, A., Dorin, T., Ivanov, R. & Sun, X. (2015). ILL-DATA 1-01-142. Institut Laue–Langevin (ILL), Grenoble, France.
De Geuser, F. & Deschamps, A. (2012). *C. R. Phys.* **13**, 246–256.
De Geuser, F., Dorin, T., Lefebvre, W., Gault, B. & Deschamps, A. (2014). *Mater. Sci. Forum*, **794–796**, 926–932.
De Geuser, F., Lefebvre, W. & Blavette, D. (2006). *Philos. Mag. Lett.* **86**, 227–234.
Deschamps, A., Bastow, T. J., de Geuser, F., Hill, A. J. & Hutchinson, C. R. (2011). *Acta Mater.* **59**, 2918–2927.
Deschamps, A. & De Geuser, F. (2011). *J. Appl. Cryst.* **44**, 343–352.
Dorin, T., Deschamps, A., Geuser, F. D. & Sigli, C. (2014). *Acta Mater.* **75**, 134–146.
Gault, B., de Geuser, F., Bourgeois, L., Gabble, B. M., Ringer, S. P. & Muddle, B. C. (2011). *Ultramicroscopy*, **111**, 683–689.
Gault, B., de Geuser, F., Stephenson, L. T., Moody, M. P., Muddle, B. C. & Ringer, S. P. (2008). *Microsc. Microanal.* **14**, 296–305.
Gault, B., Haley, D., de Geuser, F., Moody, M. P., Marquis, E. A., Larson, D. J. & Geiser, B. P. (2011). *Ultramicroscopy*, **111**, 448–457.
Gerold, V. (1977). *J. Appl. Cryst.* **10**, 25–27.
Guinier, A. (1938). *Nature*, **142**, 569–570.
Gumbmann, E., Lefebvre, W., De Geuser, F., Sigli, C. & Deschamps, A. (2016). *Acta Mater.* **115**, 104–114.
Huang, T. C., Toraya, H., Blanton, T. N. & Wu, Y. (1993). *J. Appl. Cryst.* **26**, 180–184.
Klobes, B., Staab, T. E. M., Haaks, M., Maier, K. & Wieler, I. (2008). *Phys. Status Solidi Rapid Res. Lett.* **2**, 224–226.
Larson, D. J., Prosa, T. J., Ulfig, R. M. & Humphrys, C. J. (2013). *Local Electrode Atom Probe Tomography: A User's Guide.* New York: Springer.
Lay, M. D. H., Zurob, H. S., Hutchinson, C. R., Bastow, T. J. & Hill, A. J. (2012). *Metall. Mater. Trans. A*, **43**, 4507–4513.
Lyon, O. & Simon, J. P. (1986). *Acta Metall.* **34**, 1197–1202.
Marceau, R. K. W., de Vaucorbeil, A., Sha, G., Ringer, S. P. & Poole, W. J. (2013). *Acta Mater.* **61**, 7285–7303.
Marceau, R. K. W., Qiu, C., Ringer, S. P. & Hutchinson, C. R. (2012). *Mater. Sci. Eng. A*, **546**, 153–161.
Marceau, R. K. W., Sha, G., Ferragut, R., Dupasquier, A. & Ringer, S. P. (2010). *Acta Mater.* **58**, 4923–4939.
Marceau, R. K. W., Sha, G., Lumley, R. N. & Ringer, S. P. (2010). *Acta Mater.* **58**, 1795–1805.
Marlaud, T., Deschamps, A., Bley, F., Lefebvre, W. & Baroux, B. (2010). *Acta Mater.* **58**, 4814–4826.
Miao, W. F. & Laughlin, D. E. (2000). *J. Mater. Sci. Lett.* **19**, 201–203.
Nagai, Y., Murayama, M., Tang, Z., Nonaka, T., Hono, K. & Hasegawa, M. (2001). *Acta Mater.* **49**, 913–920.
Noble, B. (1968). *Met. Sci. J.* **2**, 117–120.
Ohnuma, M., Suzuki, J., Ohtsuka, S., Kim, S.-W., Kaito, T., Inoue, M. & Kitazawa, H. (2009). *Acta Mater.* **57**, 5571–5581.
Porod, G. (1982). *Small-Angle X-ray Scattering*, edited by O. Glatter & O. Kratky, pp. 17–51. London: Academic Press.
Preston, G. (1938). *Nature*, **142**, 570.
Ringer, S. P., Hono, K., Polmear, I. J. & Sakurai, T. (1996). *Appl. Surf. Sci.* **94–95**, 253–260.
Ringer, S. P., Hono, K., Sakurai, T. & Polmear, I. J. (1997). *Scr. Mater.* **36**, 517–521.
Ringer, S. P., Quan, G. C. & Sakurai, T. (1998). *Mater. Sci. Eng. A*, **250**, 120–126.
Rosen, M., Horowitz, E., Swartzendruber, L., Fick, S. & Mehrabian, R. (1982). *Mater. Sci. Eng.* **53**, 191–198.
Somoza, A. & Dupasquier, A. (2003). *J. Mater. Process. Technol.* **135**, 83–90.
Starink, M. J. (2004). *Int. Mater. Rev.* **49**, 191–226.
Starink, M. J., Gao, N. & Yan, J. L. (2004). *Mater. Sci. Eng. A*, **387–389**, 222–226.
Sudbrack, C. K., Noebe, R. D. & Seidman, D. N. (2006). *Phys. Rev. B*, **73**, 212101.
Teubner, M. & Strey, R. (1987). *J. Chem. Phys.* **87**, 3195–3200.
Vurpillot, F., Gault, B., Geiser, B. P. & Larson, D. J. (2013). *Ultramicroscopy*, **132**, 19–30.